

## TITLE PAGE

# A Versatile Functional Interaction between Electrically Silent Kv Subunits and Kv7 Potassium Channels

Vijay Renigunta<sup>1</sup>, Nermina Xhaferri<sup>1</sup>, Imran Gousebasha Shaikh<sup>1</sup>, Jonathan Schlegel<sup>1</sup>, Rajeshwari Bisen<sup>1</sup>, Ilaria Sanvido<sup>2</sup> Theodora Kalpachidou<sup>2</sup>, Kai Kummer<sup>2</sup>, Dominik Oliver<sup>1</sup>, Michael G. Leitner<sup>2,4</sup> and Moritz Lindner<sup>1,3,4,4</sup>

<sup>1</sup>Department of Neurophysiology, Institute of Physiology and Pathophysiology, Philipps-University Marburg, 35037 Marburg, Germany

<sup>2</sup>Institute of Physiology, Medical University of Innsbruck, Innsbruck, Austria

<sup>3</sup>The Nuffield Laboratory of Ophthalmology, Sleep and Circadian Neuroscience Institute, Nuffield Department of Clinical Neurosciences, University of Oxford, Oxford, United Kingdom

<sup>4</sup>Department of Ophthalmology, Philipps University Marburg, 35037 Marburg, Germany.

<sup>4</sup> To whom correspondence should be addressed: Michael.Leitner@i-med.ac.at and Moritz@LindnerLab.de

**Running title:** Silent Kv Subunits Modulate Kv7 Currents

Number of words: 6193

Number of Figures 6

**ORCID:** ML: 0000-0002-4416-3421  
VR: 0000-0003-4123-4447  
DO: 0000-0002-8368-0923  
TK: 0000-0002-7924-7772  
KK: 0000-0002-5854-6503  
MGL: 0000-0002-3259-6481

## Funding

Supported by the German Research Foundation (LI 2846/5-1 to ML and RE 4617/2-1 to VR), the Austrian Science Fund FWF (ZFI-053640 to KK and MGL) and by research Grants of the University Medical Centre Giessen und Marburg to MGL (UKGM 13/2016) and ML (UKGM 15/2020).

## Summary

Voltage-gated K<sup>+</sup> (K<sub>V</sub>) channels govern K<sup>+</sup>-ion flux across cell membranes in response to changes in membrane potential. They are formed by the assembly of four subunits, typically from the same family. Electrically silent K<sub>V</sub> channels (K<sub>V</sub>S), however, are unable to conduct currents on their own. It has been assumed that these K<sub>V</sub>S must obligatorily assemble with subunits from the K<sub>V</sub>2 family into heterotetrameric channels, thereby giving raise to currents distinct from those of homomeric K<sub>V</sub>2 channels.

Herein, we show that K<sub>V</sub>S subunits indeed also modulate the activity, biophysical properties and surface expression of recombinant K<sub>V</sub>7 isoforms in a subunit-specific manner. Employing co-immunoprecipitation, and proximity labelling, we unveil the spatial coexistence of K<sub>V</sub>S and K<sub>V</sub>7 within a single protein complex. Electrophysiological experiments further indicate functional interaction and probably heterotetramer formation. Finally, single-cell transcriptomic analyses identify native cell types in which this K<sub>V</sub>S and K<sub>V</sub>7 interaction may occur. Our finding demonstrate that K<sub>V</sub> cross-family interaction is much more versatile than previously thought – possibly serving nature to shape potassium conductance to the needs of individual cell types.

## Introduction

Voltage-gated potassium channels (K<sub>v</sub> channels) are a diverse family of evolutionarily conserved membrane proteins that allow the flux of K<sup>+</sup> ions across cellular membranes. They play a significant role in determining the excitability of tissues including heart, skeletal muscle, brain, and retina. Based on sequence homology, mammalian K<sub>v</sub> channels are divided into 12 subfamilies (K<sub>v</sub>1–12) (Alexander *et al*, 2017). Functional K<sub>v</sub> channels are formed as tetramers of pore-forming  $\alpha$ -subunits. These may be made-up by four identical isoforms (homotetramers) or of  $\alpha$ -subunits from distinct members of the same K<sub>v</sub> subfamily (heterotetramers). Heterotetramerization across family borders is typically not possible. The only known exception to this is the heterotetramerization of K<sub>v</sub>2 channels with members of the so-called silent modifier (K<sub>v</sub>S) families, K<sub>v</sub>5, K<sub>v</sub>6, K<sub>v</sub>8, and K<sub>v</sub>9.

K<sub>v</sub>S were termed “silent”, as they are unable to form functional homotetramers at the plasma membrane on their own. When expressed alone, they are retained in intracellular compartments, without giving rise to an electrical current (Bocksteins, 2016). However, when co-expressed with K<sub>v</sub>2 subunits, they co-assemble into functional K<sub>v</sub>S/K<sub>v</sub>2 heterotetramers, with electrophysiological and pharmacological characteristics markedly different to those of K<sub>v</sub>2 channels alone (Bocksteins, 2016; Bocksteins & Snyders, 2012). Such K<sub>v</sub>2-K<sub>v</sub>S heteromerization greatly broadens the functional diversity of K<sub>v</sub>2 channels. The physiological relevance thereof is highlighted by the fact that mutations in the *KCNV2* gene, encoding K<sub>v</sub>8.2 subunits, cause *KCNV2*-associated retinopathy (Gayet-Primo *et al*, 2018; Guimaraes *et al*, 2020). In this condition, the lack of intact K<sub>v</sub>8.2 causes alterations in a conductance termed I<sub>K,x</sub>, which counterbalances the dark current in photoreceptors, to an extent that finally photoreceptor death is caused (Gayet-Primo *et al*, 2018; Hart *et al*, 2019; Smith *et al*, 2012). Similarly, variants in *KCNV1* (K<sub>v</sub>8.1) and *KCNV2* are associated with certain forms of epilepsy (Bergren *et al*, 2009; Jorge *et al*, 2011; Winden *et al*, 2015).

Structurally, the K<sub>v</sub>  $\alpha$ -subunit consists of six transmembrane domains (S1–S6) and a pore loop (between S5 and S6) with the signature sequence (TTIGYGD) determining K<sup>+</sup> selectivity. The S1–S4 region represents the voltage-sensing domain, and the cytoplasmic N- and C-termini are relevant for subunit assembly, trafficking and functional channel regulation through signalling cascades. Notably, it is well established that K<sub>v</sub>S affect K<sub>v</sub>2 currents by altering membrane trafficking, but also by modifying the voltage dependence of activation and inactivation as well

as the gating properties (Bocksteins, 2016; Bocksteins & Snyders, 2012; Stas *et al*, 2015). Tetramerization in most Kv channels, including the interaction between Kv2 and KvS, primarily occurs in the endoplasmic reticulum (ER). This process involves the primary interaction of T1 domains located in the cytoplasmic N terminus of each subunit (Tu *et al*, 1996). The exact mechanism by which the T1 domain determines subunit specificity remains poorly understood. It is worth noting that certain Kv subunits, such as the Kv7 channel families, lack the T1 domain but are still capable of forming functional homo- and heteromers (Bal *et al*, 2008; Haitin & Attali, 2008; Howard *et al*, 2007). Given the specific co-assembly of closely-related family members, it is reasonable to assume that sequence homology is an important determinant of tetramerization. In this regard, we found that KvS (with the exception of Kv5) are more closely related to members of the Kv7 family than to the other Kv subunits including Kv2 ((Gutman *et al*, 2005) and Supplementary Figure 1). We therefore hypothesised that KvS may constitute modifiers of Kv7 channels and investigated this interaction in a series of electrophysiological, molecular and cell biological experiments. We found that KvS modulate current amplitude and voltage-dependence of neuronal Kv7 isoforms in a bi-directional manner, and we present biochemical and electrophysiological evidence that Kv7 and KvS physically assemble into the same protein complex, allowing for direct interaction and possibly even heterotetramerisation.

Overall, this work reveals previously unknown ability of Kv7 and KvS to assemble into complexes with unique electrophysiological properties. This may represent a mechanism to extend the native repertoire of K<sup>+</sup> currents to maintain cell physiology in various tissues.

## Results

### ***Bi-directional modulation of Kv7 channels through KvS***

To explore the potential modulation of Kv7-mediated currents by KvS, we initiated our analyses by characterising K<sup>+</sup> currents in Chinese hamster ovary (CHO) cells transiently co-expressing Kv7.2 channel subunits together with different KvS in whole cell patch-clamp recordings. Depolarising voltage steps (-100 mV to +60 mV) induced slowly activating outwardly rectifying K<sup>+</sup> currents that were completely absent in non-transfected CHO cells and in cells expressing only KvS (not shown). Strikingly, voltage-dependent currents were significantly reduced in cells co-expressing Kv7.2 with either Kv5.1 Kv8.2, Kv9.1 or Kv9.2 subunits compared to cells expressing Kv7.2 alone (Figure 1 A, B; exemplary recordings are shown in Figure 5 B). Also, in cells co-expressing Kv7.2 with either Kv5.1, Kv8.2, Kv9.1 or Kv9.2 we observed an alteration of biophysical characteristics in that the steady-state voltage-dependence

of whole cell currents were shifted to significantly more depolarised values as compared to cells expressing Kv7.2 only. The magnitude of this shift was in the range of about +10 mV for  $V_h$  values (Figure 1 C, D). The voltage sensitivity as determined by the slope of the voltage dependence was not altered by co-expression of KvS. The smaller current amplitudes and altered voltage-dependence were accompanied by significantly more depolarised resting potentials in the cells co-expressing Kv7.2 with either Kv5.1 Kv8.2, Kv9.1 or Kv9.2 (not shown). In contrast, steady-state current amplitudes were significantly increased in cells co-expressing Kv6.1 and Kv8.1 channels without however affecting voltage dependence or membrane potentials compared to cells expressing only Kv7.2 subunits (Figure 1 A-D). Co-expression of Kv6.3, Kv6.4 or Kv9.3 did not affect the characteristics of currents through Kv7.2 channels (Figure 1 A-D).

To assess whether KvS similarly modulated the properties of currents through other Kv7 channels, we performed analogous experiments in CHO cells expressing either Kv7.4 subunits alone or together with KvS. Notably, the effects of co-expression of KvS on Kv7.4 subunits were very similar to those observed for Kv7.2 channels, except that no effect was observed for Kv5.1 and shifts in  $V_h$  were substantially more pronounced (Figure 1 E-G and Supplementary Figure 2).

Taken together, these experiments demonstrated that KvS modulated Kv7 channels in a subunit-specific manner.

### ***Kv8 and Kv7 subunits exist in multi-protein complexes in living cells***

We then turned our attention to investigating how KvS subunits modulates Kv7 channels at the molecular level, focusing on Kv8.1 and Kv8.2 subunits and analysed whether Kv7 and Kv8 subunits were present in the same protein complex and in close proximity to each other. We hence carried-out BioID and co-immunoprecipitation experiments in HEK cells. For BioID experiments, we transiently overexpressed BioID2-HA-tagged KvS (Kv8.1 or Kv8.2) and flag-tagged Kv7 subunits (Figure 2). To ensure that the BioID2 fusion did not affect the expression and subcellular localisation of the KvS subunits, we performed immunostainings on transfected HeLa cells with antibodies against the HA tag at the C-terminal end of Kv8.1, Kv8.2 BioID2 fusion proteins. This revealed the expected intracellular localisation with a signal pattern typical of the endoplasmic reticulum (ER) within the cells. (Figure 2 B; Supplementary Figure 8).

Biotinylation of endogenous proteins in cells expressing HA-BioID2-KvS (8.1 and 8.2) with exogenous biotin strongly stimulated a wide range of endogenous proteins on western blots

probed with Alexa Fluor™ 488 streptavidin conjugate (data not shown). This indicates that the BioID2 moiety was adequately exposed in the KvS fusion construct, allowing for efficient biotinylation. Our next step was to test whether the Kv7 subunits are in close proximity to the KvS subunits. If they are indeed in close proximity, they should be biotinylated and then precipitated with streptavidin beads. To achieve this, we transiently expressed BioID2 tagged KvS (8.1 or 8.2) and flag tagged Kv7.2 constructs in HEK293 cells in the presence of 50  $\mu$ M biotin for 24 h and then lysed the cells using a radio-immunoprecipitation assay (RIPA) lysis buffer. HEK293 cells transfected with BioID2-HA alone, processed in parallel, were used as negative controls. As shown in Figure 2C (anti-flag staining, green arrows), the flag-tagged Kv7.2 subunits were robustly precipitated using streptavidin beads, strongly suggesting that the Kv7.2 subunits are indeed in close proximity (10 nm distance) to the KvS (8.1 and 8.2) subunits and are therefore biotinylated, whereas no precipitation occurred when BioID2 alone was used as a negative control (red arrow). To complement these data with an independent approach, we performed a proximity ligation assay (PLA) on cells transfected with myc-tagged KvS and flag-tagged Kv7. Indeed, PLA signals were only observed in cells co-expressing both, KvS and Kv7 (Supplementary Figure 3).

We then asked whether the flag-tagged Kv7.2 was located in the same complex as the KvS subunits by carrying out co-immunoprecipitation experiments. The protein complexes were precipitated with anti-flag M2 beads, and the subunits in the precipitates were detected in western blots with antibodies directed against myc or flag tags, respectively (Figure 3 A, B). These results demonstrated that the Kv7.2 and KvS channels were not only located in close proximity, but also exist in a single multi-protein complex. As a negative control, co-immunoprecipitation experiments were carried out using Dynabeads coated with unrelated IgG antibodies and with cell lysates devoid of KCNQ subunits (Supplementary Figure 4, Supplementary Figure 5), demonstrating the specificity of co-immunoprecipitations.

### ***Kv8 modulate Kv7 currents by affecting both membrane trafficking and biophysical properties***

We then sought to determine whether KvS modulated Kv7 currents through mechanisms similar to those involved in the regulation of Kv2 channels. To this end, we measured the plasma membrane expression of both Kv7.2 and Kv7.4 channels containing an extracellular HA tag, in *Xenopus laevis* oocytes using a luminometric assay (Renigunta *et al*, 2014). This method involves the oxidation of luminol by horseradish peroxidase (HRP) in conjunction with antibodies that can detect HA-tagged Kv7 channels located on the oocyte surface. The intensity

of light emitted directly correlates with the membrane expression of Kv7 channels (Figure 4 A). In these experiments, co-expression of Kv8.1 significantly increased the membrane expression of both Kv7.2 and Kv7.4 channels, whereas co-expression of Kv8.2 slightly decreased the membrane expression of both channels (Figure 4 B, C), fully in line with the observed effects on current density (c.f., Figure 1). Taken together, these data indicated that Kv8.1 enhances Kv7 currents by increasing their membrane expression, whereas co-expression of Kv8.2 may reduce current amplitudes, at least in part, by attenuating surface expression of Kv7 channels. Therefore, we conclude that KvS modulates Kv7 currents by altering their membrane abundance, similar to the mechanisms reported for Kv2.1 channels, but, unlike Kv2 channels, in a bidirectional manner (Bocksteins, 2016; Bocksteins & Snyders, 2012).

We then set out to gain insight into whether KvS subunits modulate Kv7 channels via heterotetramerization into the same channel complex or by close interaction, e.g., as associated but independent channel entities or as some sort of ancillary beta subunit (Figure 5 A). To determine whether all isoforms contribute to the channel pore (i.e. heterotetramerization), we generated channels containing mutations in the GYG pore motif (GYG/AAA exchange for Kv8.1 and GYG/GYD exchange for Kv7.2) that render these variants inactive. When co-expressed with wild-type subunits, such variants are known to attenuate whole cell currents via dominant-negative effects (Leitner *et al*, 2012). Assuming fully stochastic co-assembly of equally available subunits, co-expression of wild-type and mutant subunits is predicted to reduce whole cell current amplitudes to 1/16 (compared to cells expressing only wild-type subunits), leaving intact a minimal number of channels containing only wild-type subunits (illustrated in Figure 5 A, first row). We performed patch-clamp recordings on cells expressing wild-type and mutant isoforms taking current densities as measure for potential co-assembly of the subunits. Co-expression of wild-type Kv8.1 with wild-type Kv7.2 significantly increased whole cell current amplitudes compared to cells expressing only Kv7.2 channels, as we had observed before (Figure 5 B). When we co-expressed pore-mutated Kv7.2(GYD) with wild-type Kv8.1, current amplitudes were reduced to virtually zero. These experiments demonstrated that Kv8.1 subunits alone were not able to form an independent functional pore (Figure 5 B).

When wild type Kv7.2 was transfected together with pore-mutated Kv8.1(AAA), current densities were reduced to approximately 50% of those observed when measuring cells transfected with both wild type constructs, resulting in current densities minimally smaller than those observed in cells transfected with Kv7.2 alone (Figure 5 B, note that amount of cDNA encoding Kv7.2 was kept constant). These results suggested that functional pore regions of

Kv8.1 are essential for KvS-dependent modulation of Kv7 channels. Noteworthy, the (only) 50% current reduction observed upon Kv8.1(AAA) co-transfection may indicate that during co-assembly Kv7.2 homotetramer formation is more likely to occur than heterotetramer formation. In particular, the 50% reduction observed herein would be expected if the probability for Kv7.2 homomers was approximately 5-fold higher than that for Kv7.2-Kv8.1 heteromers. Yet, our observations clearly rule out alternative modes of interaction: If Kv7.2 and Kv8.1 co-existed as independent channels (Figure 5 A, second row), a substantial current should have been observable upon co-expression of pore-mutated Kv7.2(GYD); If Kv8.1 was a beta-subunit to Kv7.2 (Figure 5 A, third row), mutating the “pore” sequence of Kv8.1 would not be expected to have any effect at all. Taken together, these data suggested that Kv7 and Kv8.1 subunits can likely heteromerise into functional channels with a slight preference for Kv7 homomers.

### ***Kv7 and KvS are expressed in the same organs and cells***

To investigate whether an interaction between Kv7 and KvS might be physiologically relevant, we used reverse transcription quantitative polymerase chain reaction (RT-qPCR) to examine the expression of Kv8 in three tissues, where the role of Kv7 channels is well established (Wang & Li, 2016). Indeed, we found that in hippocampus and dorsal root ganglia, the abundance of *Kcnv1* (Kv8.1) mRNA was in the same order of magnitude as that of *Kcnq2* (Kv7.2) mRNA. In both these neural tissues, also *Kcnv2* (Kv8.2) mRNA was detected, though at much lower levels (Figure 6 A). By contrast, in heart, expression levels of *Kcnv2* (Kv8.2) were comparable to those of *Kcnq1* (Kv7.1), while *Kcnv1* mRNA was not detected (Figure 6 B).

To further evaluate whether Kv7 and KvS transcripts merely coexist in the same tissue, or are actually transcribed in the same cells we analysed publicly available single-cell RNA sequencing (scRNAseq) datasets from the hippocampus (Saunders *et al*, 2018), dorsal root ganglia (DRG) (Finno *et al*, 2019) and the heart (Tabula Muris *et al*, 2018). Consistent with our observations in the qPCR experiments we found high read counts for *Kcnq2* and *Kcnv1* in hippocampal and DRG cells, whereas *Kcnv2* was barely detected. In the dataset from cardiac cells, in turn, *Kcnq1* and *Kcnv2* were predominant, whereas Kv8.1/*Kcnv1* was not found (Supplement material file 1, Table S2).

In the hippocampus, *Kcnv1* was encountered in seven clusters, with the highest transcript counts being observed in the clusters representing CA1-3 pyramidal neurons, dentate hilus and dentate principal neurons (Figure 6 C). To see if the observed transcriptomic expression pattern would also be supported by methods that provide spatially encoded information, we employed single

molecule fluorescence RNA in-situ hybridization (“RNAScope”). Indeed, using RNAScope we find *Kcnv1* expression patterns closely matching the observations made using scRNAseq (Figure 6 D-G). By far the highest *Kcnv1* signal was obtained from the CA2 region, followed by the dentate gyrus and the CA1 region. In scRNAseq, both Kv7.2/*Kcnq2* and Kv2.1/*Kcnb1* were both found in each of these cell types /clusters (Figure 6 H, Supplementary Figure 7 A). We argued that if Kv8.1 would interact with Kv7.2 rather than a Kv2 in hippocampal neurons, one would expect *Kcnv1* expression levels to correlate stronger with those of *Kcnq2* than with those of *Kcnb1* or *Kcnb2* at the single cell level. Indeed, Pearson’s correlation coefficient (PCC) for *Kcnv1* with *Kcnq2* was higher than the correlation of *Kcnv1* with 99 [98 - 99] % of all other transcripts encountered, and in particular higher than that with *Kcnb1* (Figure 6 H, left, Supplement material file 1, Table S3).

In dorsal root ganglia, *Kcnv1* and *Kcnq2* overlapped in two clusters (Supplementary Figure 7 B). In stark contrast to the hippocampus, *Kcnv1* expression levels in DRG were more strongly correlated with those of Kv2 channel genes rather than with those of Kv7 channel genes (Figure 6 H, middle, Supplement material file 1, Table S3). In the heart, *Kcnv2* was found exclusively in the cluster representing cardiac myocytes, as was *Kcnq1* (Supplementary Figure 7 C). Here, the PCC for *Kcnv2* with *Kcnq1* was higher than the correlation of *Kcnv2* with 0.99 [0.98 - 1.00] % of all transcripts encountered, and, again, particularly higher than that with *Kcnb1* (Figure 6 H, right, Supplement material file 1, Table S3). Taken together, these transcriptomic analyses suggest that Kv7 and Kv8 mRNA expression is strongly correlated within individual cells in hippocampus and heart, whereas this was not the case in the DRG.

## Discussion

In the present work, we show that Kv channels from the silent Kv-subfamily (KvS) can interact with Kv7 channels to alter their trafficking and biophysical properties. Modulation of Kv2 channels through KvS has long been reported (Bocksteins, 2016; Bocksteins & Snyders, 2012) and, up until now, this has been considered to be the only case of cross-family interaction among Kv channel families. Yet, in analogy to their actions on Kv2 channels (Bocksteins, 2016), KvS reduced Kv7-mediated currents through an alteration of Kv7 membrane targeting and voltage-dependency. Importantly, – and in contrast to their effects on Kv2 – certain KvS also increased Kv7 current amplitudes and surface expression. Thus, modulation of Kv7 by KvS is bidirectional and thereby more diverse than the modulation of Kv2. Based on our data, we hypothesise that Kv7 co-assemble with KvS into functional heteromers. This further broadens

the functional diversity of Kv channels and may serve to shape potassium conductance to fit the needs of individual cell types.

### ***Mode and functional aspects of the Kv7-KvS interaction***

Using PLA and BioID experiments, we herein demonstrated that in living cells Kv7 co-exist with Kv8.1 and Kv8.2 in close physical proximity. In addition, we could show by co-immunoprecipitation that these ion channels assemble into a common protein complex. This interaction dictates trafficking of Kv7 channels to the plasma membrane allowing for a bidirectional modulation of Kv7-mediated current amplitudes. Indeed, the enhanced surface abundance of Kv7.2 and Kv7.4 in *Xenopus laevis* oocytes upon co-expression of Kv8.1 was paralleled by increased macroscopic Kv7.2 and Kv7.4 current amplitudes recorded from CHO cells. Conversely, co-expression of Kv8.2 resulted in a reduction in both macroscopic current amplitudes and surface expression. We conclude that the molecular mechanism of the KvS-dependent modulation of Kv7 currents may be similar to that of Kv2 channels (i.e., modulation of surface expression plus modulation of biophysical properties). However, bidirectional modulation of current amplitudes indicates that the interaction between Kv7 and KvS may be somewhat more versatile than their interaction with Kv2 channels, which are generally down-regulated by KvS (Bocksteins, 2016). Taking into account our RNA-sequencing analyses, co-expression of Kv7.2 and Kv8.1 in hippocampal neurons, for example, may lead to a tuned decrease in electrical excitability by increasing the Kv7-mediated M-current (Wang *et al*, 1998). Modulation of Kv7.1 by Kv8.2 subunits in cardiac muscle, in turn, may lead to a slower and delayed repolarization process. However, mouse models carrying genetic deletions will be required to unequivocally demonstrate whether this novel interaction is also relevant in native tissues.

Although our data provide clear evidence for the coexistence of Kv7 and KvS subunits in a common protein complex, and the functional relevance of the interaction, we are unable to draw a definite conclusion as to whether Kv7 and KvS co-assemble into functional heterotetramers, as it has been previously been shown for Kv2 channels (Bocksteins *et al*, 2009; Moller *et al*, 2020). Since KvS altered voltage dependence of Kv7 channels, we propose heteromerisation also for KvS and Kv7 channels. In support of this notion, we observed that co-transfection of dominant-negative pore-mutant Kv8 with wild-type Kv7.2 led to a robust (~50%) reduction of current amplitudes as compared to transfection of both wild-type subunits, i.e., the functional modulation of Kv7.2 currents was abolished via co-expression of Kv8 pore mutants. While these findings are in line with a possible heterotetramerization, the dominant-negative effects

of KvS pore mutants on Kv7 currents were somewhat weaker than expected: Assuming each subunit would be built into a heterotetramer with equal probability a ~95 % reduction in current amplitude would be anticipated. Importantly, it is unclear whether the potential Kv7-KvS heterotetramerization is fully stochastic. Specifically, a roughly 5-fold assembly preference for respective homotetramers over heterotetramers would explain the observed 50% current reduction. Potential preference for homomers over heteromer formation might seem surprising, but it has indeed been demonstrated even for the well-studied Kv2-Kv8.2 interaction, and the degree of current reduction observed for Kv2.1 by dominant-negative Kv8.2 mutants is only slightly higher than what we observed in our study (Czirjak *et al*, 2007; Smith *et al.*, 2012). Nevertheless, there is still room for debate regarding the mode of interaction and studying Kv7.4 channels (where changes in the  $V_h$  upon co-transfection of dominant-negative KvS) or on Kv7-KvS concatamers may help to clarify this issue in future.

### ***The physiological role of Kv7-KvS interaction***

In the present study, we used a wide variety of cell types, including cell lines from primates, rodents and amphibian origin. This substantiates the notion that the interaction between Kv7 and KvS is not restricted to a particular species or cell line, but instead represents a universally observable and evolutionarily stable phenomenon.

To further explore the presence of Kv7-KvS interaction in native systems, we delved into where this interaction might occur. Through RT-qPCR analysis, we detected the expression of Kv8.1 and Kv8.2 in three tissues, where Kv7 play a well-established, prominent role (Greene & Hoshi, 2017; Maljevic *et al*, 2008): the hippocampus, dorsal root ganglia, and the heart (Figure 6 A - C). We then analysed single-cell RNA-sequencing datasets, and observed that Kv7 and KvS were not just expressed in the same tissues, but actually in the same cell types and cells (Supplementary Figure 7). Moreover, we found that on the level of individual cells, in several subtypes of hippocampal neurons (e.g. CA1-CA3) and cardiac muscle cells expression levels of Kv7 and KvS were robustly correlated. Furthermore, our analysis revealed that in the hippocampus and heart, the expression of Kv8.1 and Kv8.2, respectively, showed a substantially stronger correlation with Kv7 as compared to Kv2. Correlation in transcript counts obviously do not immediately proof functional interaction on protein level. Thus, these findings fall short in providing direct evidence for a functional Kv7-KvS interaction in the examined tissues. Recent studies, however, show that transcript-level correlation is commonly maintained on protein level and can help to predict protein function (Ribeiro *et al*, 2022; Sharan *et al*, 2007).

To establish definitive evidence for the presence of Kv7-KvS complexes in native tissues and unravel their physiological significance, further investigations encompassing both structural and functional studies are warranted. Specifically, functional studies present significant challenges that can only be addressed by establishing knockout mouse models and/or a comprehensive pharmacological characterization of Kv7/KvS complexes. In this regard, it is encouraging that a first Kv8.2 mouse model is available and has been partially characterized (Hart *et al.*, 2019; Jiang *et al*, 2021). These approaches will clarify the specific roles and functional properties of Kv7-KvS interactions in biological systems.

### ***Translational relevance***

While this is primarily a cell physiological study, the herein-described Kv7-KvS interaction may hold promise for clinical and translational applications. The newfound Kv7-KvS complex may pose unique pharmacological properties that are distinct from Kv7 complexes not encompassing KvS. This would enable the development of pharmacological agents specifically targeting Kv7-KvS complexes while leaving Kv7 homotetramers unaffected. Such an approach could enable highly specific pharmacotherapies e.g. for epilepsy or cardiac arrhythmias.

Indeed, before persuading such translational directions a better understanding of the role of Kv7-KvS complexes in native tissues as well as their pharmacological properties is required.

### ***Conclusion***

In summary, our study provides evidence for the formation of a common protein complex between KvS and Kv7 subunits. These complexes exhibit distinct electrophysiological properties, possibly through heterotetramer formation. Our data, suggest that such interactions may also occur in native tissues, particularly in the hippocampus and the heart. KvS-Kv7 interactions could therefore represent a mechanism utilized by nature to further increase the functional diversity of Kv channels and to fine-tune the electrophysiological properties of individual cell types to their functional needs.

## MATERIAL AND METHODS

### *Animal studies*

Adult female African clawed frogs (*Xenopus laevis*) were used for experiments with *Xenopus* oocytes. The frogs were anaesthetized by placing them in water containing 1 g/l tricaine. Stage V oocytes were collected from the ovarian lobes. Anesthesia and surgery were performed with the approval of the Giessen Regional Animal Health Authority.

C57Bl/6J mice were purchased from Janvier Labs (Le Genest-Saint-Isle, France). Tissue collection was performed in accordance with the Ethics Guidelines of Animal Care (Medical University of Innsbruck).

### *Molecular cloning and mutagenesis*

Supplemental Table S1 summarizes the constructs used in this study. QuikChange II XL Site-Directed Mutagenesis Kit (Stratagene, Agilent Technologies, Waldbronn, Germany) was utilized to introduce point mutations. To enhance expression efficiency, all constructs utilized for experiments in *Xenopus* oocytes were subcloned between the 5' and 3' UTR of the *Xenopus*  $\beta$ -globin gene in the modified pSGEM vector. The mMessage mMachine kit (Ambion, Huntingdon, UK) was used to synthesize complementary RNA transcripts. For surface quantification assays, a plasmid containing KCNQ2 (Schwake *et al*, 2003) or KCNQ4 (HJ Kim *et al*, 2011) with an external hemagglutinin (HA) epitope tag was used. All DNA constructs were verified through Sanger sequencing.

### *Cell Culture and Transfection*

Chinese hamster ovary (CHO) dhFR<sup>-</sup> cells were maintained as previously described (Lindner *et al*, 2011). In brief, cells were kept in MEM Alpha Medium supplemented with 10% fetal calf serum (FCS) and 1% penicillin/streptomycin (Invitrogen GmbH, Darmstadt, Germany) in a humidified atmosphere at 5% CO<sub>2</sub> and 37°C. Cells were transiently transfected with jetPEI transfection reagent (Polyplus Transfection, Illkirch, France). HeLa and HEK cells were cultured in the same way as CHO. Transfection of HeLa cells was performed using jetPRIME transfection reagent (Polyplus Transfection, Illkirch, France).

### *Electrophysiological Recordings*

Whole-cell recordings were performed on transiently transfected CHO cells in culture, as previously reported (Leitner *et al*, 2011; Leitner *et al*, 2018; Wilke *et al*, 2014). All experiments

were performed approximately 48 h after transfection at room temperature (22°C-25°C) (Dierich *et al*, 2020). During recordings, cells were kept in extracellular solution containing (in mM): 144 NaCl, 5.8 KCl, 1.3 CaCl<sub>2</sub>, 0.7 Na<sub>2</sub>HPO<sub>4</sub>, 0.9 MgCl<sub>2</sub>, 5.6 glucose, 10 HEPES, pH adjusted to 7.4 (NaOH) (305-310 mOsm/kg). Whole-cell patch clamp recordings were performed at room temperature (19-23°C) with an HEKA EPC10 USB patch clamp amplifier controlled by PatchMaster software (HEKA, Lambrecht, Germany) or an Axopatch 200B amplifier (Molecular Devices, Union City, CA). Voltage clamp recordings were low-pass filtered at 2.5 kHz and sampled at 5 kHz. Recordings were excluded from analyses, when the series resistance (R<sub>s</sub>) was  $\geq 7 \text{ M}\Omega$ , and R<sub>s</sub> was compensated through-out the recordings to 80%, with the exception of the data presented in Figure 5, where no R<sub>s</sub> compensation was performed. Patch pipettes were pulled from borosilicate glass (Sutter Instrument Company, Novato, CA, USA) and had a resistance of 2-3.5 MΩ after filling with intracellular solution containing (mM): 135 KCl, 3.5 MgCl<sub>2</sub>, 2.4 CaCl<sub>2</sub> (0.1 free Ca<sup>2+</sup>), 5 EGTA, 5 HEPES and 2.5 Na<sub>2</sub>-ATP (pH adjusted with KOH to 7.3; 290-295 mOsm/kg).

### ***Co-immunoprecipitation***

To perform immunoprecipitations, anti-FLAG M2 magnetic beads from Sigma-Aldrich (St. Louis, MO) were used in accordance with the manufacturer's instructions. Briefly, lysates from HEK293 cells that expressed flag-tagged Kv7 and myc-tagged KvS were utilized. The beads were coated with antibody and then incubated with the cell lysates under rotation at 4°C for 12 hours. Beads with antigen-antibody complex were extensively washed (4 times) with wash buffer, followed by elution of the proteins on the beads through boiling at 72°C for 10 minutes in 2 x SDS sample loading buffer. The proteins were then separated on a 10-12% SDS-PAGE under reducing conditions, transferred to a nitrocellulose membrane and probed with either a mouse anti-myc antibody (1:1000; Cell Signaling, Danvers, MA) or a monoclonal ANTI-FLAG® M2 antibody (1:1000; Sigma-Aldrich). Fluorescent secondary antibodies (1:5000; Bio-Rad, Hercules, CA) were used to visualize the membrane, which was then imaged with a ChemiDoc MP imaging system from Bio-Rad.

### ***Proximity Ligation Assay***

CHO cells were fixed in 4% ice-cold methanol-free paraformaldehyde as previously described (Lindner *et al*, 2020). Proximity ligation assay (PLA) was performed using the Duolink *In-Situ* Red Starter Kit (Sigma-Aldrich) according to the manufacturer's protocol, with the amplification step being performed by incubation with polymerase at 37°C for 50 minutes.

Primary antibodies used were rabbit anti myc (71D10, Cell Signaling) at a dilution of 1:200 and mouse anti flag (F1804, Sigma-Aldrich) at 1:400. Fluorescent secondary antibody (Alexa 488 conjugated Donkey anti mouse, ThermoFisher, Waltham, USA, 1:250) was added during the PLA probe incubation step. Image acquisition was performed using an LSM710 confocal laser scanning microscope (LSM, Carl Zeiss, Jena, Germany) as previously described (Lindner *et al.*, 2020).

### ***BioID Proximity-Dependent Biotinylation assay***

K<sub>v</sub>S -BioID2 (HA tag and BirA R118G mutant fused to the C-terminus of K<sub>v</sub>S subunits) was transfected into 6 cm plates of HEK293 cells. After 24 hours of transfection, 50 µM biotin was added to the culture medium to induce biotinylation of proteins in the vicinity of BioID2- K<sub>v</sub>S in the cells for 18-24 hours. Cells were lysed in RIPA lysis buffer (150 mM NaCl; 50 mM Tris HCl pH=7.4; 1% Triton X100; 0.1% SDS; 0.5% sodium deoxycholate). The sample was passed through an 18-gauge needle several times to reduce viscosity. Biotinylated proteins were purified using streptavidin-agarose (Pierce/Thermo Fisher) and eluted in 6x SDS-PAGE sample buffer containing 3 mM biotin by boiling at 95 °C for 10 min under reducing conditions. Proteins were transferred to a nitrocellulose membrane and probed with either a flag tag monoclonal antibody (1:1000; Proteintech, Rosemont, IL) or Alexa Fluor™ 488 streptavidin conjugate (1:3000; Invitrogen, Watham, MA) for detection of biotinylated proteins.

### ***Single molecule fluorescence in situ hybridization***

Brains were rapidly extracted from C57Bl/6J mice and flash-frozen in isopentane on dry ice. Brains were then coronally sectioned at 14 µm thickness in a cryostat. Sections were air-dried for 20 min and subsequently stored at -80 °C until used. The RNAscope Multiplex Fluorescent v2 Assay (Advanced Cell Diagnostics, Newark, CA, USA) was used to visualize mRNA expression following the manufacturer's instructions except for the washings steps that were extended to 10 min. *Kcnv1* mRNA was detected using the target probe Mm-Kcnv1 (Advanced Cell Diagnostics) and the Opal™ 650 dye (1:1500, Akoya Biosciences, Marlborough, MA, USA)

### ***Surface Quantification Assay***

The surface expression of HA-tagged K<sub>v</sub>7 subunits in Xenopus oocytes was analysed 2 days after injection of the cRNA (10 ng/oocyte of HA-tagged K<sub>v</sub>7.2 alone or together with 10 ng/oocyte of K<sub>v</sub>8.1 or K<sub>v</sub>8.2). To block non-specific antibody binding, oocytes were incubated in ND96 (in mM: NaCl 96, KCl 2, CaCl<sub>2</sub> 1.8, MgCl<sub>2</sub> 1, HEPES 20, Na-pyruvate 2.5, and

100U/ml Penicillin-streptomycin) solution containing 1% Bovine serum albumin (BSA) at 4 °C for 30 min. Oocytes were then incubated for 60 min at 4 °C with 100 µg/ml rat monoclonal anti-HA antibody (clone 3F10, Roche Pharmaceuticals, Basel, Switzerland) in 1% BSA/ND96, washed 6 times at 4 °C with 1% BSA/ND96 and incubated with 2 µg/ml of peroxidase-conjugated, affinity-purified, F(ab)2-fragment goat anti-rat immunoglobulin G antibody (Jackson ImmunoResearch, West Grove, PA) in 1% BSA/ND96 for 60 min. Oocytes were washed thoroughly, first in 1% BSA/ND96 (4°C, 60 min) and then in 1x ND96 without BSA (4 °C, 15 min). Individual oocytes were placed in 20 µL of SuperSignal Elisa Femto solution (Pierce, Chester, UK) and, after an equilibration period of 10 s, chemiluminescence was quantified in a luminometer (Lumat LB9507, Berthold Technologies, Bad Wildbad, Germany). For each construct, the surface expression of 20 oocytes was analysed in one experiment and at least three experiments (~40 oocytes) were performed. The luminescence produced by uninjected oocytes was used as a negative control.

### ***Quantitative reverse transcriptase-PCR***

DRG, hippocampus and heart tissue were isolated from C57Bl/6J mice, snap frozen in liquid nitrogen and stored at -80°C until use. RNA extraction and reverse transcription quantitative polymerase chain reaction (RT-qPCR) were performed as previously described (Kalpachidou *et al*, 2022; Kummer *et al*, 2018). Briefly, the peqGOLD TriFast reagent (Peqlab) was used to extract total RNA according to manufacturer's instructions [chloroform (C2432) and absolute ethanol (107017) were obtained from Merck]. RNA pellets were reconstituted in nuclease free water (R0582, ThermoFisher Scientific) and concentration was measured using NanoDrop 2000 (ThermoFisher Scientific). Reverse transcription was performed using MuLV reverse transcriptase (N8080018, ThermoFisher Scientific) according to the supplier's protocol. Gene expression was estimated using the following TaqMan Gene Expression Assays (ThermoFisher Scientific): Kcnq1 (Mm00434640\_m1), Kcnq2 (Mm00440080\_m1), Kcnv1 (Mm00550691\_m1), Kcnv2 (Mm00807577\_m1), Hprt (Mm00446968\_m1), Sdha (Mm01352363\_m1), and Tfrc (Mm00441941\_m1), with Hprt, Sdha and Tfrc serving as reference genes. Reactions were prepared according to TaqMan Gene Expression Assays protocol (20µL reactions), loaded on MicroAmp Fast Optical 96-well reaction plates (ThermoFisher Scientific) and run on the 7500 Fast Real-Time PCR System (Thermo Fisher Scientific). The protocol details were as follows: an initial 10 min 95 °C step, followed by 40 two-step cycles of 15 s at 95 °C and 1 min at 60 °C. Samples (eight per tissue) were run as technical duplicates alongside non-template controls. Threshold was set manually at 0.1,

whereas baselines were estimated automatically.  $C_q$  values for each sample were normalized to the respective geometric mean of the  $C_q$  values of the three reference genes (Hprt/Sdha/Tfrc) and subsequently expressed in relation to the average expression of either Kcnq2 (for DRG and hippocampus tissues) or Kcnq1 (for heart tissue).

### ***Data analysis and statistics***

Patch clamp recordings were analysed with PatchMaster (HEKA) and IgorPro (Wavemetrics, Lake Oswego, OR) or R version 4.1.5 (RCoreTeam, 2014) together with the PatchR package (<https://github.com/moritzlindner/PatchR>). Voltage dependence of activation was derived from tail current amplitudes using voltage protocols indicated: Maximal amplitudes of tail currents were fit with a two-state Boltzmann function with  $I = I_{\min} + (I_{\max}-I_{\min})/(1 + \exp((V-V_h)/s))$ , where  $I$  is current,  $V$  is the membrane voltage,  $V_h$  is the voltage at half maximal activation, and  $s$  describes the steepness of the curve. Results on voltage dependence are shown as normalised tail current (conductance)-voltage curves, obtained by normalizing to  $(I_{\max}-I_{\min})$ , obtained from fits to data of individual experiments. Statistical analysis was performed with two-tailed Student's, Wilcoxon signed, Dunnett or Scheffé test as appropriate. For surface expression analysis in oocytes, values from three experiments were normalised to oocytes injected with extracellularly HA-tagged Kv7 cRNA. Statistical analysis was carried out by ordinary one-way ANOVA with post hoc Dunnett's multiple comparison test. Statistical significance was assigned at  $P \leq 0.05$  (\*  $P \leq 0.05$ , \*\*  $P \leq 0.01$ , \*\*\*  $P \leq 0.001$ ). All data are presented as mean  $\pm$  SEM. In electrophysiological experiments,  $n$  represents the number of individual cells recorded from at least three independent experiments (independent transfections or independent tissue, i.e. biological replicates).

Confocal micrographs from PLA experiments were analysed using FIJI (National Institutes of Health, Bethesda, MD, USA, (Schindelin *et al*, 2012)) and a custom-made macro (accessible via: [https://www.kvs-liaison.eu/data/PLA\\_Macro\\_autothreshold.ijm](https://www.kvs-liaison.eu/data/PLA_Macro_autothreshold.ijm)). This macro enabled unbiased analysis of the micrographs by automatically (1) detecting the boundaries of cells showing flag immunofluorescence, and (2) then counting the PLA dots inside and outside the boundaries of those immunopositive cells separately. Summary statistics were then performed using R version 4.1.5 (RCoreTeam, 2014) and ggplot2 (Wickham H., 2016).

### ***Bioinformatics***

Three individual published single-cell RNA sequencing datasets were utilized to analyse the distribution and co-expression of Kv8, Kv7 and Kv2 in hippocampus (Saunders *et al.*, 2018),

dorsal root ganglia (DRG, (Finno *et al.*, 2019)) and heart (Tabula Muris *et al.*, 2018), respectively. Raw gene count matrices were obtained from the Genome Expression Omnibus (GEO) archive (DRG: GSE128276) or author curated archives (hippocampus: dropviz.org, heart:

[https://figshare.com/projects/Tabula\\_Muris\\_Transcriptomic\\_characterization\\_of\\_20\\_organisms\\_and\\_tissues\\_from\\_Mus\\_musculus\\_at\\_single\\_cell\\_resolution/27733](https://figshare.com/projects/Tabula_Muris_Transcriptomic_characterization_of_20_organisms_and_tissues_from_Mus_musculus_at_single_cell_resolution/27733)). Processing and analysis of the datasets were performed using R 4.1.5 and Seurat 3.1 (Usoskin *et al*, 2015). Data were log-normalized, centred, and scaled. Where available, cluster assignments lists as published by the authors of the datasets were utilized. For DRG, clustering was performed using the KNN and Louvain algorithms implemented in Seurat after regressing out technical variance. Obtained clusters were validated using a set of unique cluster markers kindly provided by the authors and the DRG cell-type marker genes as reported by Usoskin et al (Usoskin *et al.*, 2015) (Supplementary Figure 6). Dot plots for Kv7, Kv2 and KvS expression in the individual cell clusters identified in each dataset were drawn with dot radius representing the percentage of cells in an individual cluster expressing the Kv or KvS gene under investigation and dot colour indicating the mean scaled gene count in that cluster, Kv/ KvS genes detected in less than 10% of the cells belonging to any individual clusters were not visualized. Finally, correlation of the expression levels of KvS with Kv7 and Kv2 were analysed using Pearson's correlation coefficients (PCC). Data were bootstrapped (n=100, with cells being individual observations) to obtain an estimate of variance. Data are presented as Box-and-Whisker plots with hinges representing quartiles and whiskers extending to the last data point within the 1.5-fold inter quartile ranges. To explore the biological plausibility of this approach correlation coefficients were also calculated for genes of ion-channels that are known to interact with any of the Kv-channels under investigation (Supplementary Figure 7 D).

## REFERENCES

Alexander SP, Striessnig J, Kelly E, Marrion NV, Peters JA, Faccenda E, Harding SD, Pawson AJ, Sharman JL, Southan C *et al* (2017) THE CONCISE GUIDE TO PHARMACOLOGY 2017/18: Voltage-gated ion channels. *Br J Pharmacol* 174 Suppl 1: S160-S194

Bal M, Zhang J, Zaika O, Hernandez CC, Shapiro MS (2008) Homomeric and heteromeric assembly of KCNQ (Kv7) K<sup>+</sup> channels assayed by total internal reflection fluorescence/fluorescence resonance energy transfer and patch clamp analysis. *J Biol Chem* 283: 30668-30676

Bergren SK, Rutter ED, Kearney JA (2009) Fine mapping of an epilepsy modifier gene on mouse Chromosome 19. *Mamm Genome* 20: 359-366

Bocksteins E (2016) Kv5, Kv6, Kv8, and Kv9 subunits: No simple silent bystanders. *J Gen Physiol* 147: 105-125

Bocksteins E, Labro AJ, Mayeur E, Bruyns T, Timmermans JP, Adriaensen D, Snyders DJ (2009) Conserved negative charges in the N-terminal tetramerization domain mediate efficient assembly of Kv2.1 and Kv2.1/Kv6.4 channels. *J Biol Chem* 284: 31625-31634

Bocksteins E, Snyders DJ (2012) Electrically silent Kv subunits: their molecular and functional characteristics. *Physiology (Bethesda)* 27: 73-84

Czirjak G, Toth ZE, Enyedi P (2007) Characterization of the heteromeric potassium channel formed by kv2.1 and the retinal subunit kv8.2 in Xenopus oocytes. *J Neurophysiol* 98: 1213-1222

Dierich M, Altoe A, Koppelman J, Evers S, Renigunta V, Schafer MK, Naumann R, Verhulst S, Oliver D, Leitner MG (2020) Optimized Tuning of Auditory Inner Hair Cells to Encode Complex Sound through Synergistic Activity of Six Independent K(+) Current Entities. *Cell Rep* 32: 107869

Finn CJ, Peterson J, Kang M, Park S, Bordbari MH, Durbin-Johnson B, Settles M, Perez-Flores MC, Lee JH, Yamoah EN (2019) Single-Cell RNA-seq Reveals Profound Alterations in Mechanosensitive Dorsal Root Ganglion Neurons with Vitamin E Deficiency. *iScience* 21: 720-735

Gayet-Primo J, Yaeger DB, Khanjian RA, Puthussery T (2018) Heteromeric KV2/KV8.2 Channels Mediate Delayed Rectifier Potassium Currents in Primate Photoreceptors. *J Neurosci* 38: 3414-3427

Greene DL, Hoshi N (2017) Modulation of Kv7 channels and excitability in the brain. *Cell Mol Life Sci* 74: 495-508

Guimaraes TAC, Georgiou M, Robson AG, Michaelides M (2020) KCNV2 retinopathy: clinical features, molecular genetics and directions for future therapy. *Ophthalmic Genet* 41: 208-215

Gutman GA, Chandy KG, Grissmer S, Lazdunski M, McKinnon D, Pardo LA, Robertson GA, Rudy B, Sanguinetti MC, Stuhmer W *et al* (2005) International Union of Pharmacology. LIII.

Nomenclature and molecular relationships of voltage-gated potassium channels. *Pharmacol Rev* 57: 473-508

Haitin Y, Attali B (2008) The C-terminus of Kv7 channels: a multifunctional module. *J Physiol* 586: 1803-1810

Hart NS, Mountford JK, Voigt V, Fuller-Carter P, Barth M, Nerbonne JM, Hunt DM, Carvalho LS (2019) The Role of the Voltage-Gated Potassium Channel Proteins Kv8.2 and Kv2.1 in Vision and Retinal Disease: Insights from the Study of Mouse Gene Knock-Out Mutations. *eNeuro* 6

Howard RJ, Clark KA, Holton JM, Minor DL, Jr. (2007) Structural insight into KCNQ (Kv7) channel assembly and channelopathy. *Neuron* 53: 663-675

Jiang X, Rashwan R, Voigt V, Nerbonne J, Hunt DM, Carvalho LS (2021) Molecular, Cellular and Functional Changes in the Retinas of Young Adult Mice Lacking the Voltage-Gated K(+) Channel Subunits Kv8.2 and K2.1. *Int J Mol Sci* 22

Jorge BS, Campbell CM, Miller AR, Rutter ED, Gurnett CA, Vanoye CG, George AL, Jr., Kearney JA (2011) Voltage-gated potassium channel KCNV2 (Kv8.2) contributes to epilepsy susceptibility. *Proc Natl Acad Sci U S A* 108: 5443-5448

Kalpachidou T, Malsch P, Qi Y, Mair N, Geley S, Quarta S, Kummer KK, Kress M (2022) Genetic and functional evidence for gp130/IL6ST-induced transient receptor potential ankyrin 1 upregulation in uninjured but not injured neurons in a mouse model of neuropathic pain. *Pain* 163: 579-589

Kummer KK, Kalpachidou T, Mitric M, Langeslag M, Kress M (2018) Altered Gene Expression in Prefrontal Cortex of a Fabry Disease Mouse Model. *Front Mol Neurosci* 11: 201

Leitner MG, Feuer A, Ebers O, Schreiber DN, Halaszovich CR, Oliver D (2012) Restoration of ion channel function in deafness-causing KCNQ4 mutants by synthetic channel openers. *British Journal of Pharmacology* 165: 2244-2259

Leitner MG, Halaszovich CR, Oliver D (2011) Aminoglycosides Inhibit KCNQ4 Channels in Cochlear Outer Hair Cells via Depletion of Phosphatidylinositol(4,5)bisphosphate. *Molecular Pharmacology* 79: 51-60

Leitner MG, Hobiger K, Mavranti A, Feuer A, Oberwinkler J, Oliver D, Halaszovich CR (2018) A126 in the active site and TI167/168 in the TI loop are essential determinants of the substrate specificity of PTEN. *Cell Mol Life Sci*

Lindner M, Gilhooley MJ, Palumaa T, Morton AJ, Hughes S, Hankins MW (2020) Expression and Localization of Kcne2 in the Vertebrate Retina. *Invest Ophthalmol Vis Sci* 61: 33

Lindner M, Leitner MG, Halaszovich CR, Hammond GR, Oliver D (2011) Probing the regulation of TASK potassium channels by PI4,5P(2) with switchable phosphoinositide phosphatases. *J Physiol* 589: 3149-3162

Maljevic S, Wuttke TV, Lerche H (2008) Nervous system KV7 disorders: breakdown of a subthreshold brake. *J Physiol* 586: 1791-1801

Moller L, Regnier G, Labro AJ, Blunck R, Snyders DJ (2020) Determining the correct stoichiometry of Kv2.1/Kv6.4 heterotetramers, functional in multiple stoichiometrical configurations. *Proc Natl Acad Sci U S A* 117: 9365-9376

RCoreTeam (2014) R: A Language and Environment for Statistical Computing. R Foundation for Statistical Computing, Vienna, Austria; 2014.

Renigunta V, Fischer T, Zuzarte M, Kling S, Zou X, Siebert K, Limberg MM, Rinne S, Decher N, Schlichthorl G *et al* (2014) Cooperative endocytosis of the endosomal SNARE protein syntaxin-8 and the potassium channel TASK-1. *Mol Biol Cell* 25: 1877-1891

Ribeiro DM, Ziyani C, Delaneau O (2022) Shared regulation and functional relevance of local gene co-expression revealed by single cell analysis. *Commun Biol* 5: 876

Saunders A, Macosko EZ, Wysoker A, Goldman M, Krienen FM, de Rivera H, Bien E, Baum M, Bortolin L, Wang S *et al* (2018) Molecular Diversity and Specializations among the Cells of the Adult Mouse Brain. *Cell* 174: 1015-1030 e1016

Schindelin J, Arganda-Carreras I, Frise E, Kaynig V, Longair M, Pietzsch T, Preibisch S, Rueden C, Saalfeld S, Schmid B *et al* (2012) Fiji: an open-source platform for biological-image analysis. *Nat Methods* 9: 676-682

Schwake M, Jentsch TJ, Friedrich T (2003) A carboxy-terminal domain determines the subunit specificity of KCNQ K<sup>+</sup> channel assembly. *EMBO Rep* 4: 76-81

Sharan R, Ulitsky I, Shamir R (2007) Network-based prediction of protein function. *Mol Syst Biol* 3: 88

Smith KE, Wilkie SE, Tebbs-Warner JT, Jarvis BJ, Gallasch L, Stocker M, Hunt DM (2012) Functional analysis of missense mutations in Kv8.2 causing cone dystrophy with supernormal rod electroretinogram. *J Biol Chem* 287: 43972-43983

Stas JI, Bocksteins E, Labro AJ, Snyders DJ (2015) Modulation of Closed-State Inactivation in Kv2.1/Kv6.4 Heterotetramers as Mechanism for 4-AP Induced Potentiation. *PloS one* 10: e0141349

Tabula Muris C, Overall c, Logistical c, Organ c, processing, Library p, sequencing, Computational data a, Cell type a, Writing g *et al* (2018) Single-cell transcriptomics of 20 mouse organs creates a Tabula Muris. *Nature* 562: 367-372

Tu L, Santarelli V, Sheng Z, Skach W, Pain D, Deutsch C (1996) Voltage-gated K<sup>+</sup> channels contain multiple intersubunit association sites. *J Biol Chem* 271: 18904-18911

Usoskin D, Furlan A, Islam S, Abdo H, Lonnerberg P, Lou D, Hjerling-Leffler J, Haeggstrom J, Kharchenko O, Kharchenko PV *et al* (2015) Unbiased classification of sensory neuron types by large-scale single-cell RNA sequencing. *Nat Neurosci* 18: 145-153

Wang HS, Pan Z, Shi W, Brown BS, Wymore RS, Cohen IS, Dixon JE, McKinnon D (1998) KCNQ2 and KCNQ3 potassium channel subunits: molecular correlates of the M-channel. *Science* 282: 1890-1893

Wang JJ, Li Y (2016) KCNQ potassium channels in sensory system and neural circuits. *Acta Pharmacol Sin* 37: 25-33

Wickham H. (2016) ggplot2: Elegant Graphics for Data Analysis. *Springer-Verlag New York*

Wilke BU, Lindner M, Greifenberg L, Albus A, Kronimus Y, Bunemann M, Leitner MG, Oliver D (2014) Diacylglycerol mediates regulation of TASK potassium channels by Gq-coupled receptors. *Nature communications* 5: 5540

Winden KD, Bragin A, Engel J, Geschwind DH (2015) Molecular alterations in areas generating fast ripples in an animal model of temporal lobe epilepsy. *Neurobiol Dis* 78: 35-44

## Author Contributions

*Participated in research design:* VR, DO, MGL, ML

*Conducted experiments:* VR, NX, IGS, JS, RB, IS, KK, MGL, ML

*Performed data analysis:* VR, NX, IGS, JS, RB, IS, KK, MGL, ML

*Wrote or contributed to the writing of the manuscript:* VR, KK, MGL, ML

## Acknowledgements

The authors acknowledge the kind gift of plasmids (K<sub>v</sub>S channels) from Regina Preisig-Müller and Elke Bocksteins and thank Olga Ebers for outstanding technical assistance.

## Declaration of Interest

MGL is employed by Boehringer Ingelheim Pharma GmbH & Co. KG (this study is not linked to this employer).

ML has received Grants from Bayer Healthcare outside the submitted work.

The other authors declare no competing interests.

## Figures

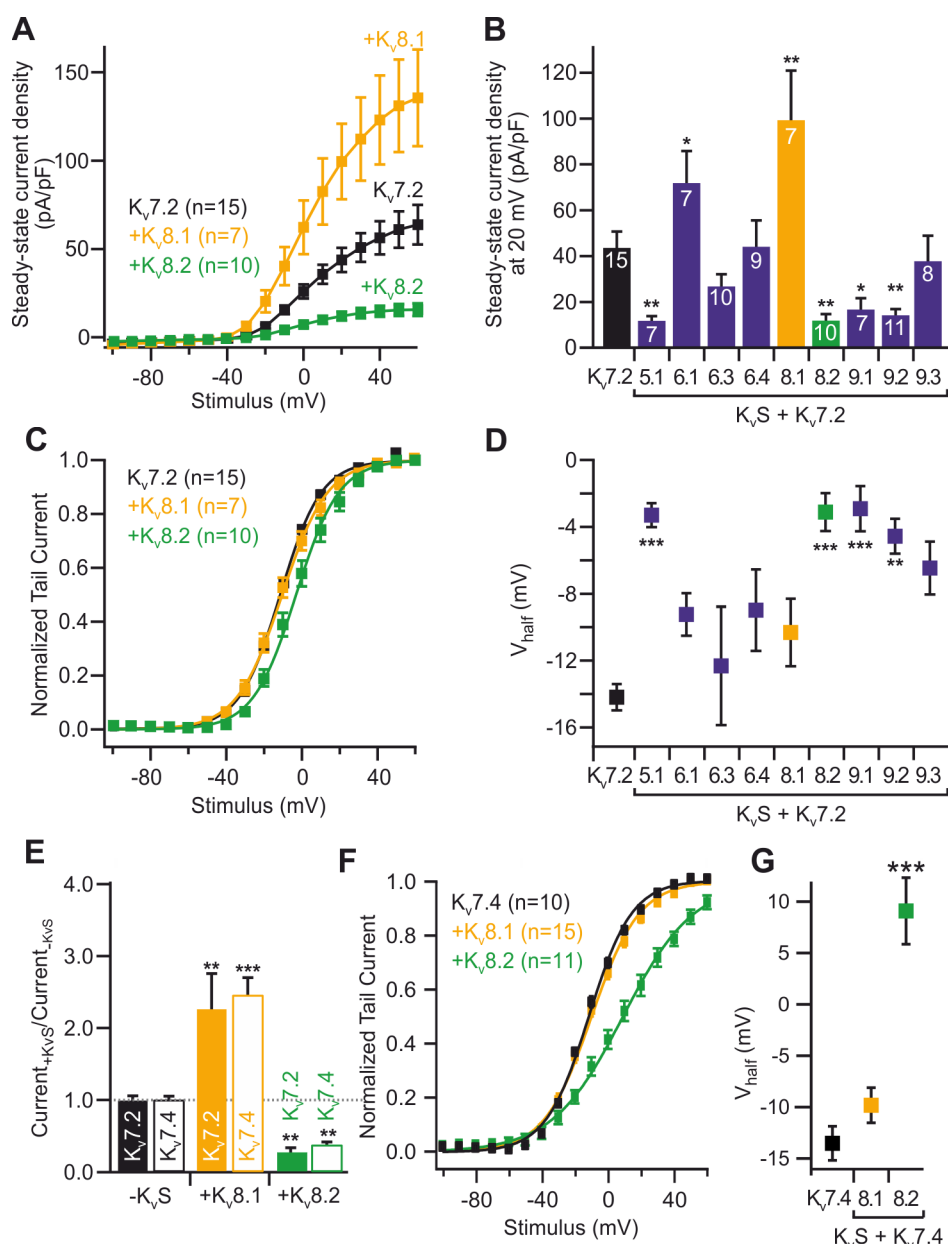


**Figure 1: Electrophysiological properties of CHO cells expressing Kv7 channels are altered by co-expression of KvS. (A)** Voltage-dependent current densities in cells expressing  $K_v7.2$  alone (black), and together with  $K_v8.1$  (orange) or  $K_v8.2$  (green). **(B)** Summary statistics for steady-state current densities at +20mV obtained in recordings similar to those shown in (A) for cells co-expressing  $K_v7.2$  together with the indicated KvS. **(C)** Normalized tail currents and half-maximal activation voltage **(D)** as deduced from Boltzmann fits (solid lines in C) for the same cells as shown in A and B. **(E)** Steady-state current densities at +20mV for  $K_v7.2$  (solid bars) or  $K_v7.4$  (empty bars) co-transfected with the indicated KvS. Data are shown as relative current densities normalized to the mean of current densities observed when  $K_v7.2$  or  $K_v7.4$  were transfected alone (" $-K_vS$ "). **(F)** Normalized tail currents and **(G)** half-maximal activation voltage as deduced from Boltzmann fits (solid lines in F) for cells expressing  $K_v7.4$  alone (black) or together with the indicated KvS.

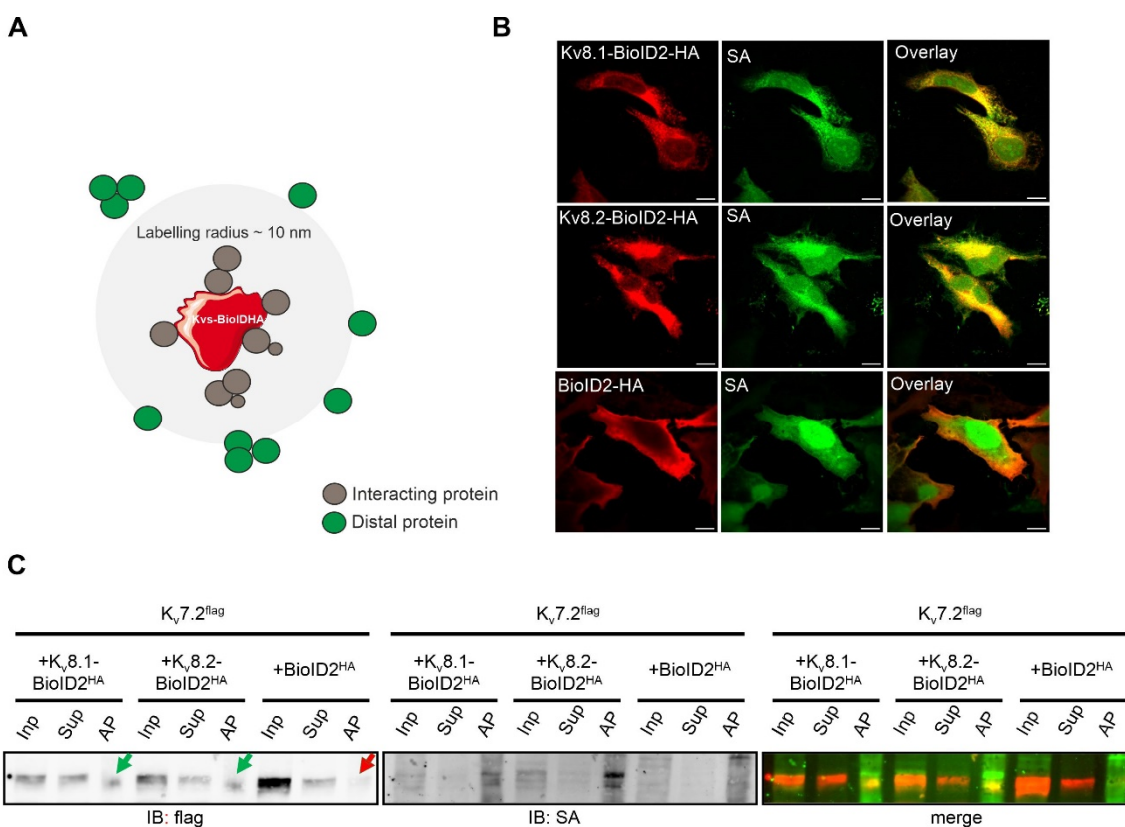


**Figure 2: Kv7 and KvS assemble in close proximity.** **(A)** BioID assay methodology. The Kv7 (8.1 / 8.2) was fused to the promiscuous form (BirA\*) of the bacterial biotin ligase BirA and co-expressed with flag tagged Kv7.2 subunits in HEK293 cells. Upon the addition of biotin, proximal proteins (grey) were biotinylated within a labeling radius of  $\sim 10$  nm, whereas the distal proteins (green), remained unlabelled. **(B)** Representative confocal images of HEK293 cells transiently transfected with BioID2-HA tagged Kv8.1 (first row), BioID2-HA tagged Kv8.2 (second row), BioID2-HA alone (third row). Cells were stained with either HA antibody (red, first column) or Alexa Fluor™ 488 streptavidin conjugate (green, second column). Scale bar, 10  $\mu$ m. **(C)** Following biotin labelling, cells were lysed and biotinylated proteins were then purified using streptavidin beads and identified by western blot analysis. Immunoblotting (IB) was performed by using an anti-flag antibody to detect the flag-labelled Kv7.2 subunits and an Alexa Fluor™ 488 streptavidin conjugate (SA) to detect the biotinylated proteins. Note the absence of flag tagged Kv7.2 subunits in the affinity purified (AP) lane with BioID2-HA alone (indicated by red arrow). However, they are present in both the (AP) lanes (indicated by green arrows). Overlaying the signals obtained from anti-flag and streptavidin staining revealed a noticeable proximity of these distinct bands (merge). Similar results were obtained in  $n = 3$  transfections.

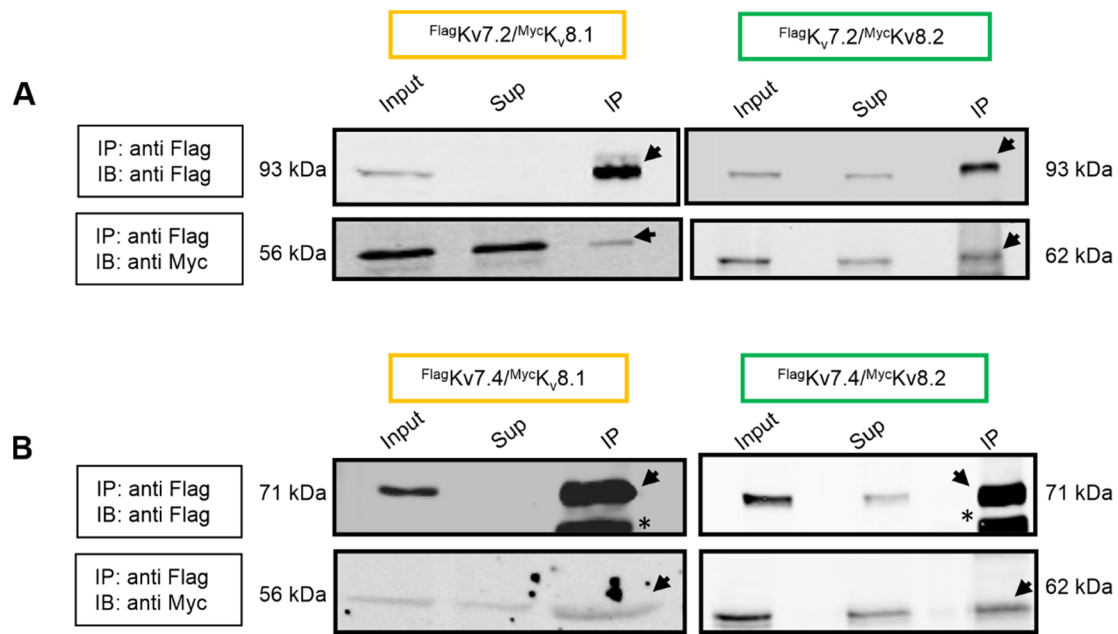


**Figure 3: Kv7 and KvS assemble into a protein complex.** Co-immunoprecipitation experiments were performed using myc-tagged Kv8.1 (left) and Kv8.2 (right) subunits in combination with flag-tagged Kv7.2 (A) and Kv7.4 (B) channel subunits from HEK293 cell lysates using monoclonal anti-flag M2 conjugated agarose beads. The precipitate was then subjected to western blot analysis using monoclonal anti-flag M2 flag antibody and anti-myc antibodies respectively. Note the presence of both Kv7 and KvS subunits in the precipitated fraction (indicated by black arrows). Asterisks indicate heavy chains detected by secondary antibodies. Abbreviations used: IP (immunoprecipitation), Sup (supernatant), IB (immunoblotting). Similar results were obtained in  $n = 3$  transfections.

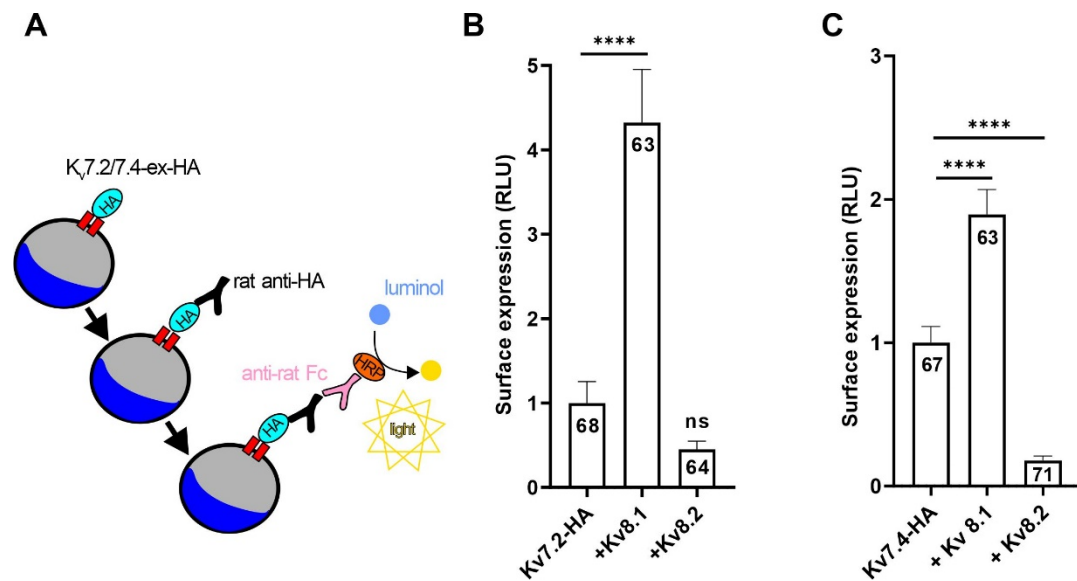


**Figure 4: Kv7 and KvS form heteromers with altered membrane trafficking.** (A) Surface expression of HA-tagged Kv7 channels measured with a luminometric technique in Xenopus oocytes. Mean surface expression of (B) HA-tagged Kv7.2 channels (C) HA-tagged Kv7.4 channels (measured in relative light units [RLUs]) in Xenopus oocytes after injection of HA-tagged Kv7 cRNA either alone or together with Kv8.1 or Kv8.2. Uninjected oocytes were used as negative control.

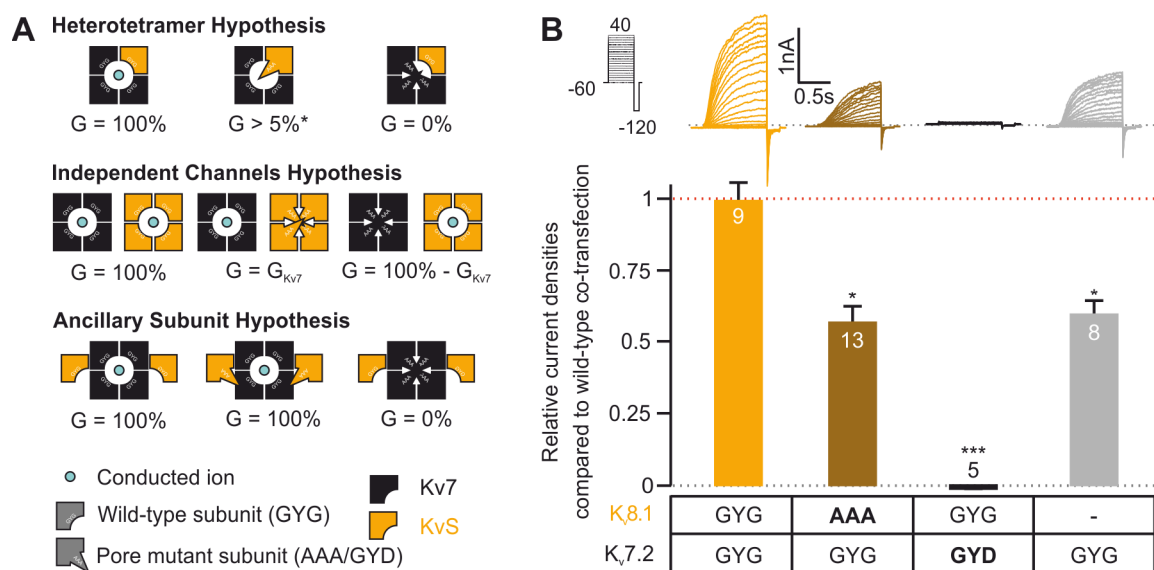


**Figure 5: Kv7 and KvS form heteromers with a single conducting pore.** **(A)** Imaginable modes of interaction of Kv7 with KvS, consequences of expression of pore mutant subunits and expected membrane conductance. \*) The percentage of current reduction depends on the probability of inclusion of the pore-mutant subunit into a heterotetramer. Detailed explanation is given in the main text. **(B)** Patch-clamp recordings from cells co-transfected with either combination of wild-type (GYG) and pore-mutated (AAA, GYD, resp.) Kv8.1 and Kv7.2 or with Kv7.2 alone. Top panel shows stimulus protocol (black) and exemplary recordings. Bottom panel shows summary statistics for steady-state current densities at +20mV. Data are shown as relative current densities normalized to the mean of current densities observed when transfected wild-type Kv7.2 with wild type Kv8.1.

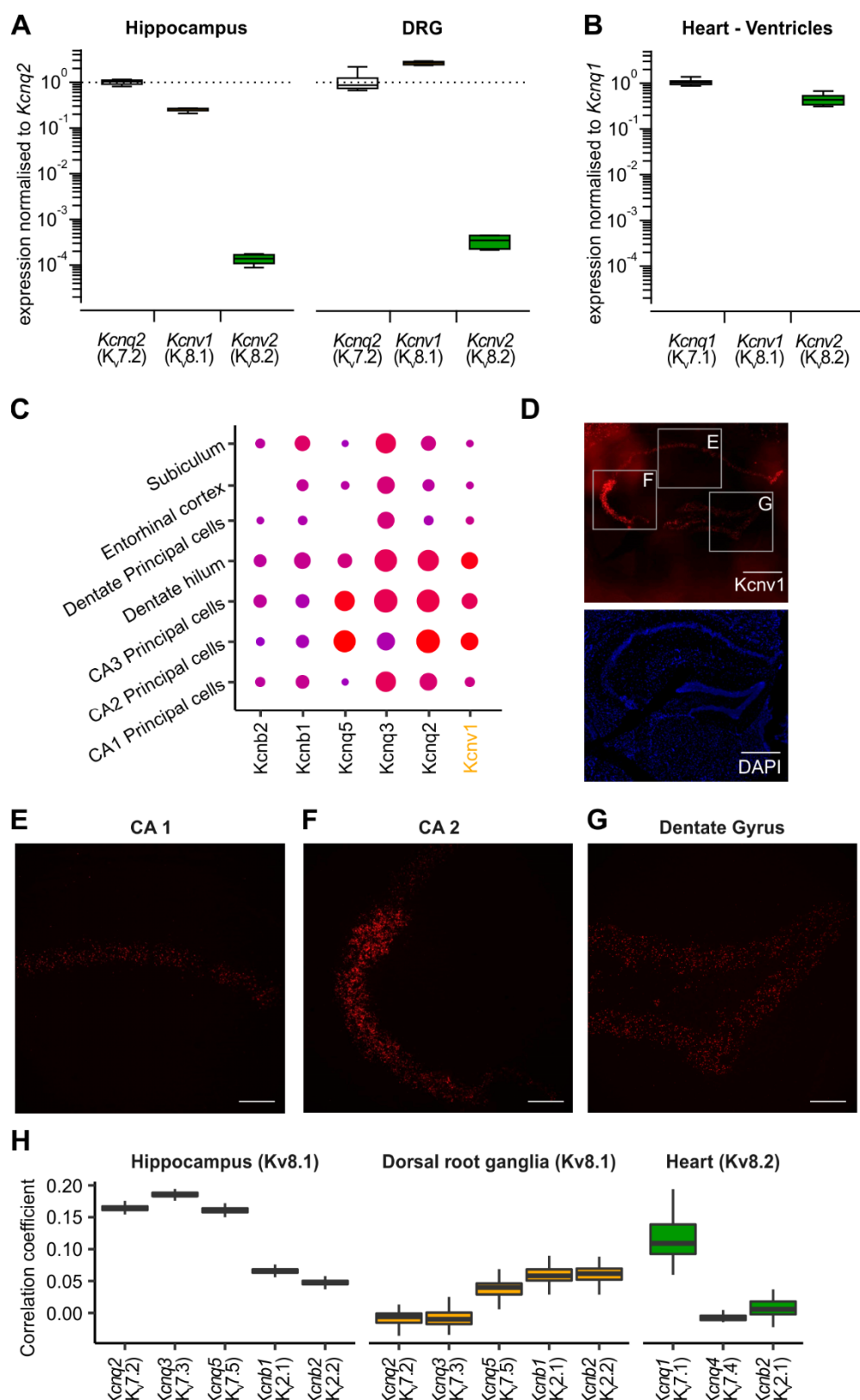


**Figure 6: Kv7 and KvS co-express in various tissues in a cell specific manner.** (A, B) Reverse transcription quantitative PCR for Kv7 and KvS transcripts from neuronal (A) and cardiac (B) tissue. For each condition 8 biological replicates with two technical replicates were included into the analysis. Shown are expression levels normalized to the mean expression level of Kv7.2 for Hippocampus and Dorsal Root Ganglia (DRG) (A) and Kv7.1 for Heart (B), respectively. (C) Expression dot plots of Kv8.1, Kv7 and Kv2 genes, for comparison, in Hippocampus. Shown are only clusters with Kv8.1 expression. The complete dot plot is given in Supplementary Figure 7. (D-G) RNAScope of Kv8.1 in the mouse hippocampus. (D) Low-magnification overview. Scale bar: 500  $\mu$ m. (E-G) High-magnification confocal micrographs of CA 1 (E), CA 2 (F) regions and Dentate Gyrus (G), respectively. Scale bar:

100  $\mu$ m. (H) Correlation coefficients for the single-cell expression of Kv7 and Kv2 with Kv8.1 or Kv8.2, respectively. Shown are Pearson's correlation coefficients for log2+1-transformed transcript counts from individual cells as observed in three publicly available single-cell RNA sequencing datasets. Included into the analysis were only cell types found to express the respective KvS.